nature geoscience

LETTERS

PUBLISHED ONLINE: 16 NOVEMBER 2015 | DOI: 10.1038/NGEO2586

Link between plate fabric, hydration and subduction zone seismicity in Alaska

Donna J. Shillington[1]*, Anne Bécel[1], Mladen R. Nedimović[2], Harold Kuehn[2], Spahr C. Webb[1], Geoffrey A. Abers[3], Katie M. Keranen[3], Jiyao Li[1], Matthias Delescluse[4] and Gabriel A. Mattei-Salicrup[5†]

Subduction zones worldwide exhibit remarkable variation in seismic activity over short distances of about tens of kilometres along their length. The properties of the subducting oceanic plate are believed to influence this seismic behaviour. However, comparisons between seismicity and plate attributes such as thermal structure made over large scales of hundreds of kilometres typically yield poor correlations[1,2]. Here we present results from controlled-source seismic data collected offshore of the Alaska Peninsula. We find that fabric in the subducting oceanic plate—the orientation and style of remnant faults originally created at the mid-ocean ridge—can contribute to abrupt changes in faulting and hydration of the plate during bending before subduction. Variations in fabric, bending faulting and hydration correlate with changes in seismicity throughout the subduction zone. More interplate and intermediate-depth intraplate earthquakes are observed where the pre-existing fabric is aligned with the trench and there is more bend faulting and hydration. This suggests that pre-existing structures in the subducting plate are an important control on abrupt variations in deformation and plate hydration and on globally observed short-wavelength variations in seismicity at subduction zones.

The subduction zone off the Alaska Peninsula exhibits major along-strike variations in the earthquake rupture history[3], present-day geodetic locking[4], and the abundance of seismicity at all depths (Fig. 1). This includes seismicity occurring on the main thrust zone where great earthquakes nucleate (interplate events) and earthquakes at larger depths within the subducting plate (intermediate-depth intraplate events). The Semidi segment ruptures in great earthquakes every ~50–75 years and seems to be geodetically locked at present, whereas the Shumagin Gap has not ruptured in a great earthquake for at least ~150 years, and may be creeping[3,4]. The Shumagin Gap exhibits abundant interplate and intermediate-depth intraplate earthquakes, and a double seismic zone is observed[5]. In contrast, the Semidi segment exhibits far sparser seismicity both at greater depths and within the plate boundary, even though great earthquakes historically occur here[3] (Fig. 1). Despite the considerable variability in seismic behaviour, the large-scale characteristics are relatively uniform along this portion of the subduction zone. The 50–55-million-year-old Pacific Plate subducts orthogonally beneath the North American Plate at ~63 millimetres per year (mm yr^{-1}; ref. 6), resulting in a uniform thermal regime. The upper continental plate consists of Tertiary and Cretaceous accreted terranes[7].

Although the large-scale plate geometry and thermal structure of the subduction zone vary little along the Alaska Peninsula, the incoming oceanic lithosphere exhibits abrupt along-strike structural changes caused by tectonic reorganizations during the entrapment of the Kula Plate from 56 to 40 million years ago. The direction and spreading rate of oceanic crust accretion varies[8] resulting in changes in the orientation and style of pre-existing structures in the plate with respect to the trench[9]. Fabric produced at the Kula–Pacific ridge at fast spreading rates (half spreading rate ~70 mm yr^{-1}) is aligned within 10°–25° of the trench at the Shumagin segment, whereas fabric produced at the Kula–Farallon ridge at intermediate spreading rates (half rate ~24 mm yr^{-1}) is highly oblique (up to 70°) to the trench at the Semidi segment (Fig. 1c).

Here we present a linkage between remnant structures in the downgoing plate, short-wavelength variations in deformation and hydration at the outer rise, and patterns of seismicity throughout the subduction zone. Our results are based on multichannel seismic (MCS) reflection, ocean-bottom seismometer (OBS) wide-angle reflection/refraction, and bathymetric data acquired off the Alaska Peninsula by the RV *Marcus G. Langseth* in July–August 2011 during the ALEUT (Alaska Langseth Experiment to Understand the megaThrust) programme.

The MCS data yield images of faulting within the sediments and upper crust, and wide-angle seismic data constrain the compressional (P-) wave speed within the crust and upper mantle, which is related to rock composition (Fig. 2). MCS and bathymetric data reveal large changes in the style and amount of bend-related faulting in the incoming plate. Outboard of the Shumagin Gap, there is pronounced bending faulting, with normal-fault offsets up to ~250 m at the sea floor and larger offsets of sediments and the igneous basement at depth (Fig. 2a,b and Supplementary Fig. 2). Faults are spaced at ~1.5 to 5 km, dip steeply both trenchward and seaward, and have average slip rates up to ~1 mm yr^{-1}. Imaged bending faults are concentrated within ~50–60 km of the trench and have strikes that are predominantly parallel to pre-existing ridge fabric, which is within ~10°–25° of the trench orientation (Fig. 1a and Supplementary Fig. 3). A smaller population of faults are parallel to the trench and slightly oblique to pre-existing fabric and may be newly formed faults; these faults have smaller throws than those that parallel pre-existing fabric (Supplementary Fig. 3). The greater number of bend faults aligned with pre-existing structures and the larger throws on these faults suggest that pre-existing fabric is a primary control on bending faulting. In contrast, the downgoing plate outboard of the Semidi segment exhibits much less

[1]Lamont-Doherty Earth Observatory of Columbia University, Palisades, New York 10964, USA. [2]Dalhousie University, Halifax, Nova Scotia B3H 4R2, Canada. [3]Cornell University, Ithaca, New York 14853, USA. [4]Laboratoire de géologie de l'ENS—PSL Research University—CNRS UMR 8538, Paris, France. [5]University of Oklahoma, Norman, Oklahoma 73019, USA. †Present address: Schlumberger Geosolutions, 10,001 Richmond Avenue, Houston, Texas 77042, USA. *e-mail: djs@ldeo.columbia.edu

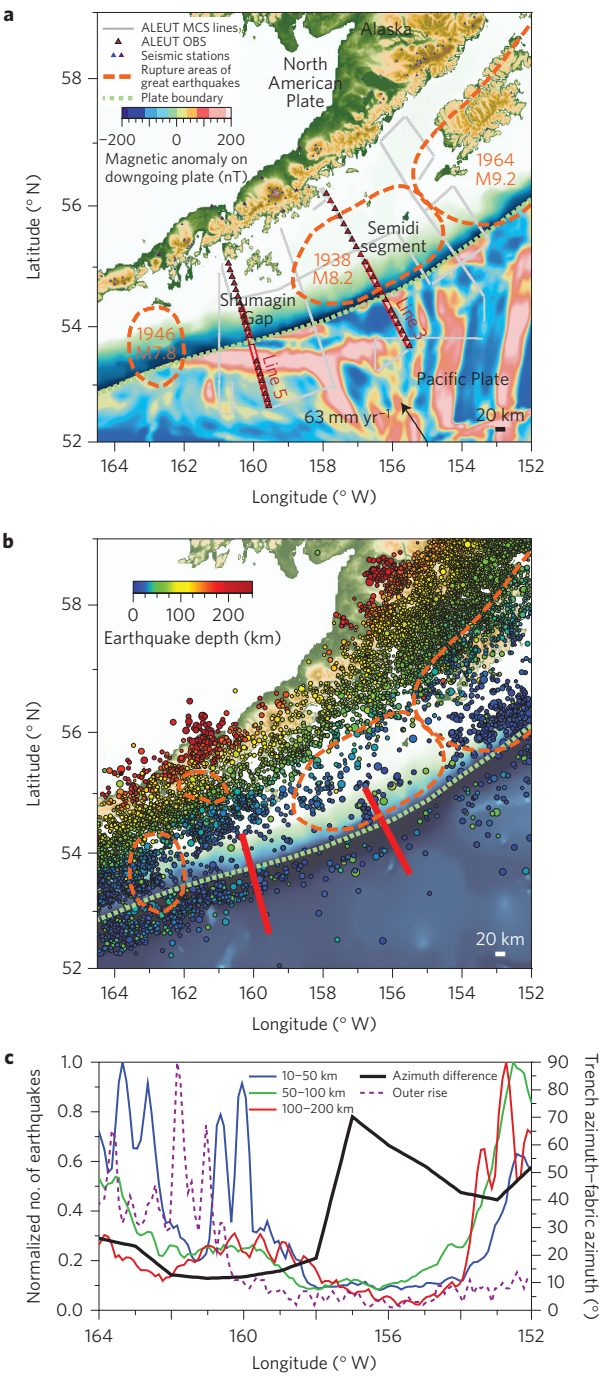

Figure 1 | Fabric in the subducting plate and seismicity in the Alaska Peninsula subduction zone. a, ALEUT experiment with bathymetry/elevation on the overriding plate and magnetic anomalies[29] on the subducting plate. The plate boundary is taken from ref. 30 and rupture zones from ref. 3. The red lines show the extent of the velocity models in Fig. 2. **b**, Seismicity from the Alaska Earthquake Information Center (AEIC) from 1990 to the present. **c**, Number of earthquakes within a 1°-wide moving window north of the trench oriented in the convergence direction and normalized by the largest number of earthquakes observed in that depth interval within our study area.

bend-related faulting. Small normal faults with maximum seafloor offsets of <30 m and orientations that are highly oblique (~70°) to the trench are observed (Fig. 2d,e); these most likely represent differential compaction of sediments across basement topography as observed farther seaward[9].

Outer-rise earthquakes are also more abundant in the Shumagin Gap than in the Semidi segment (Fig. 1c), which provides further support for variations in the amount and style of bending deformation. These results strongly suggest that favourably oriented pre-existing structures are important in controlling the formation of bending faults. Similar correlations between the abundance of bending faulting and favourably oriented pre-existing structures are observed in other subduction zones[10–12]. Other factors are likely to contribute to variations in bend faulting, including changes in megathrust coupling within the subduction zone[13,14] and/or changes in curvature of the plate. However, we consider pre-existing structures to be one of the primary controls given the abrupt change in bending faulting and its correlation to changes in fabric orientation.

P-wave velocity models derived from wide-angle seismic data suggest that changes in bending faulting are accompanied by changes in hydration of the oceanic plate. Bending faults constitute the primary pathways for water to penetrate into oceanic crust and upper mantle away from the mid-ocean ridge[12]. In the Shumagin Gap, where bend faulting is abundant, a reduction in upper mantle velocity from 8.25 to <7.75 km s^{-1} is observed within the uppermost 3–4 km of the mantle (Fig. 2c). We interpret this velocity reduction as evidence for the formation of the hydrous mineral serpentine, consistent with similar patterns in other subduction zones[15,16]. If this velocity change is solely explained by hydration, it implies serpentinization of at least ~16 wt% or ~1.8 wt% H_2O (refs 17,18). Other factors may contribute to the reduction in upper mantle velocity, including porosity created by faulting. The velocities in the upper crust also decrease in the bending area, which is most likely due to fractures, fluids and/or hydrous minerals. The oceanic crust and upper mantle off the Semidi segment exhibit more heterogeneous crustal and upper mantle velocity structure, possibly because this line obliquely crosses crust produced at intermediate spreading rates. However, no comparable reduction in velocities is observed in the uppermost mantle nearing the trench, implying much less hydration, which is consistent with the paucity of faults at the outer rise to deliver water into the plate (Fig. 2f), as also observed elsewhere[19].

Along-strike variations in bending faulting and hydration offshore of the Alaska Peninsula strongly correlate with variations in the abundance of interplate and intermediate-depth earthquakes (Fig. 1). The Shumagin segment is characterized by much more abundant intermediate-depth and interplate seismicity than the Semidi segment in all depth ranges on the basis of local and global earthquake catalogues (Fig. 1c and Supplementary Fig. 14). There are several different mechanisms by which the downgoing plate may exert a control on both intermediate-depth earthquakes and interplate earthquakes.

Many previous studies attribute intermediate-depth intraplate seismicity to dehydration embrittlement, where the dehydration of mineral-bound water within the downgoing plate causes elevated pore fluid pressures, thus enabling seismic slip at temperatures and pressures where ductile deformation should normally occur[20]. The depth at which mineral-bound water is released is controlled by the thermal structure of the subducting plate and the minerals in which water is stored[2,21]. Except at discontinuities in plate age, the thermal structure changes along-strike over several hundreds of kilometres, and thus cannot explain observed changes in the abundance of intermediate-depth earthquakes over tens of kilometres. In this study area, more water enters the subduction zone at the Shumagin Gap than the Semidi segment largely owing to favourably oriented remnant structures, and thus more water is available to drive dehydration embrittlement and possibly intermediate-depth seismicity here. Dehydration reactions are expected to occur at depths up to ~190–200 km on the basis of the modelled thermal structure and expected hydrous minerals[21], which matches the

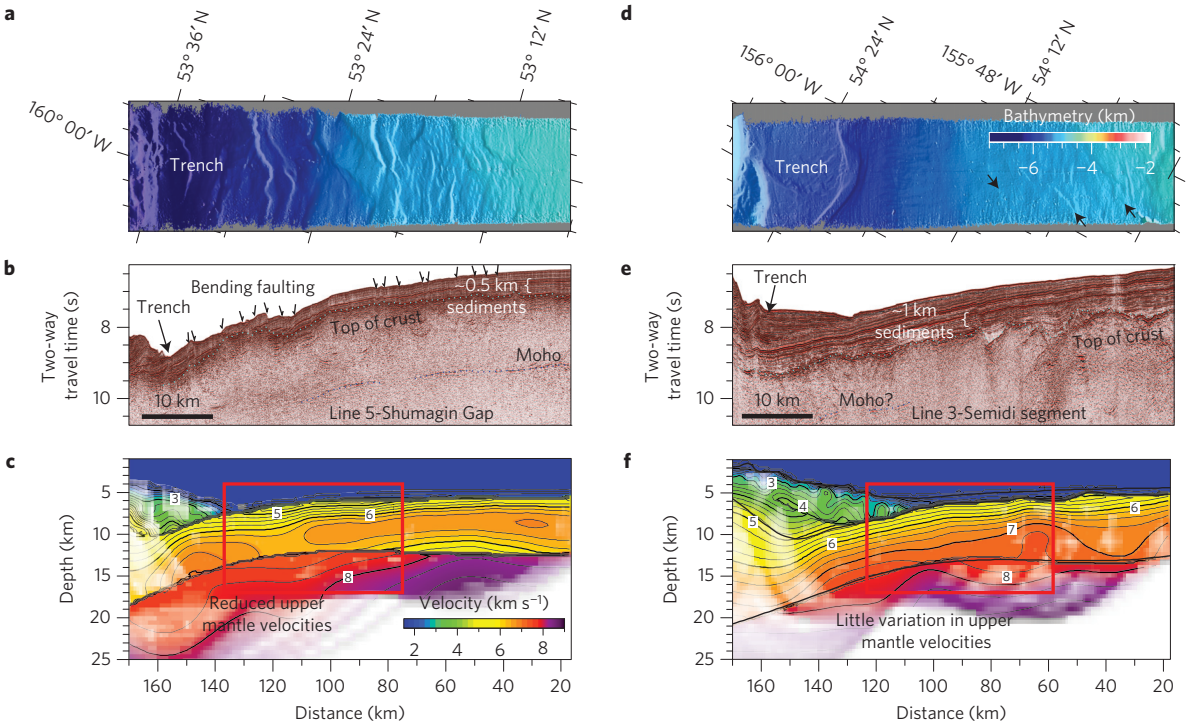

Figure 2 | Comparison of bending faulting and hydration between the Shumagin Gap and Semidi segment. a–f, Illuminated seafloor multibeam bathymetry (**a**,**d**), multichannel seismic reflection profiles (**b**,**e**), and P-wave velocity structure (**c**,**f**). P-wave velocity models in **c** and **f** are masked by the density of ray coverage. The red rectangles in **c** and **f** show the extent of the plotted regions in **a**,**b**,**d**,**e**. The small black arrows in **d** indicate surface expression of small faults on ALEUT Line 3. The arrows in **b** show a subset of interpreted bending faults.

observed depth extent of intermediate-depth seismicity (Fig. 1). Although the thermal structure of the Semidi segment should be nearly identical, fewer intermediate-depth earthquakes occur here perhaps because less mineral-bound water is present to dehydrate. Global correlations are generally poor between intermediate-depth earthquakes and the depth ranges at which dehydration reactions are expected on the basis of the assumption that a constant amount of water is stored in the crust and upper mantle[1,2]. However, these correlations do not take into account varying hydration of the plate described here.

A related mechanism proposed for intermediate-depth earthquakes is the re-activation of bending faults[22,23], by, for example, viscous shear instabilities[24] or dehydration. Such faults form zones of weakness and are favourably oriented with respect to stresses in the slab. Limited focal mechanisms show down-dip extension beneath the Alaska Peninsula[5]. The larger abundance of faults in the subducting plate in the Shumagin Gap compared with the Semidi segment that are oriented favourably with respect to the expected stress field at depth may explain variations in intermediate-depth earthquakes. In either case, the orientation of pre-existing structures in the downgoing plate with respect to the trench seems to have a controlling influence on intermediate-depth seismicity.

Topography and sediments at the top of the downgoing plate and faulting and hydration of the upper crust could also contribute to along-strike changes in interplate seismicity[25,26]. Abundant interplate micoseismicity is observed in the Shumagin Gap, where a faulted basement with relatively thin (0.5 km) sediment cover is subducting. Once subducted, such irregularities on the plate may promote localized areas of higher coupling[26], and rupture in a series of small earthquakes. The subducting plate in the relatively quiet Semidi segment contains basement ridges formed during intermediate rate spreading[9], but these are blanketed by >1 km of sediment, which may result in a relatively smooth, lubricated contact at depth and thus in more distributed, even coupling and less seismicity but a contact capable of rupturing more easily in great ($M > 8$) earthquakes[25]. Many other factors also are likely to contribute to variations in interplate seismicity, particularly variations in coupling; creeping sections of faults often exhibit higher levels of seismicity[27]. Furthermore, the thickness and lithology of sediments delivered into the subduction zone, dewatering of the sediments, upper and lower crust, and the distribution of fluids along the plate boundary will also influence plate boundary properties and seismic behaviour[28]. However, our results suggest that variations in roughness at the top of subducting plate due to bend faulting are one important contribution to interplate seismicity.

Observations from offshore of the Alaska Peninsula demonstrate that inherited structures in the oceanic plate exert a powerful influence on processes throughout the subduction zone, from faulting and hydration at the outer rise to seismicity at depth. Abrupt along-strike variations in plate hydration, such as those observed here, can regulate the quantity of water delivered into the subduction zone. This has consequences not only for intermediate-depth earthquakes, but also for the composition and volume of island arc magmatism and the global water budget in the deep Earth[2]. Most global studies of the impact of water on subduction zone processes assume uniform plate hydration[1,2,21]; our work demonstrates that plate hydration can vary at scales of tens of kilometres. Understanding controls on seismicity throughout the subduction zone is also essential for a broader understanding of seismic behaviour and seismic hazards in subduction zones.

Methods

Methods and any associated references are available in the online version of the paper.

Received 30 May 2015; accepted 13 October 2015; published online 16 November 2015

References

1. Barcheck, C. G., Wiens, D. A., van Keken, P. E. & Hacker, B. R. The relationship of intermediate- and deep-focus seismicity to the hydration and dehydration of subduction slabs. *Earth Planet. Sci. Lett.* **349,** 153–160 (2012).
2. Hacker, B. R. H_2O subduction beyond arcs. *Geochem. Geophys. Geosyst.* **9,** Q03001 (2008).
3. Davies, J., Sykes, L., House, L. & Jacob, K. Shumagin seismic gap, Alaska Peninsula: History of great earthquakes, tectonic setting, and evidence for high seismic potential. *J. Geophys. Res.* **86,** 3821–3855 (1981).
4. Fournier, T. J. & Freymueller, J. T. Transition from locked to creeping subduction in the Shumagin region, Alaska. *Geophys. Res. Lett.* **34,** L06303 (2007).
5. Abers, G. A. Relationship between shallow- and intermediate-depth seismicity in the eastern Aleutian subduction zone. *Geophys. Res. Lett.* **19,** 2019–2022 (1992).
6. Sella, G. F., Dixon, T. H. & Mao, A. REVEL: A model for recent plate velocities from space geodesy. *J. Geophys. Res.* **107,** ETG 11-1–ETG 11-30 (2002).
7. Plafker, G., Moore, J. C. & Winkler, G. R. in *The Geology of Alaska* (eds Plafker, G. & Berg, H. C.) 389–449 (Geological Society of America, 1994).
8. Lonsdale, P. Paleogene history of the Kula plate: Offshore evidence and onshore implications. *Geol. Soc. Am. Bull.* **10,** 733–754 (1988).
9. Bécel, A., Shillington, D. J., Nedimović, M. R., Webb, S. C. & Kuehn, H. Origin of dipping structures in fast-spreading oceanic lower crust offshore Alaska imaged by multichannel seismic data. *Earth Planet. Sci. Lett.* **424,** 26–37 (2015).
10. Kobayashi, K., Nakanishi, M., Tamaki, K. & Ogawa, Y. Outer slope faulting associated with the western Kuril and Japan trenches. *Geophys. J. Int.* **134,** 356–372 (1998).
11. Masson, D. G. Fault patterns at outer trench walls. *Mar. Geophys. Res.* **13,** 209–225 (1991).
12. Ranero, C. R., Phipps Morgan, J., McIntosh, K. & Reichert, C. Bending-related faulting and mantle serpentinization at the Middle America trench. *Nature* **425,** 367–373 (2003).
13. Christensen, D. H. & Ruff, L. J. Seismic coupling and outer rise earthquakes. *J. Geophys. Res.* **93,** 13421–413444 (1988).
14. Emry, E. L., Wiens, D. A. & Garcia-Castellanos, D. Faulting within the Pacific plate at the Mariana Trench: Implications for plate interface coupling and subduction of hydrous minerals. *J. Geophys. Res.* **119,** 3076–3095 (2014).
15. Ivandic, M., Grevemeyer, I., Berhorst, A., Flueh, E. R. & McIntosh, K. Impact of bending related faulting on the seismic properties of the incoming oceanic plate offshore of Nicaragua. *J. Geophys. Res.* **113,** B05410 (2008).
16. Fujie, G. *et al.* Systematic changes in the incoming plate structure at the Kurile trench. *Geophys. Res. Lett.* **40,** 88–93 (2013).
17. Christensen, N. I. Serpentinites, peridotites, and seismology. *Int. Geol. Rev.* **46,** 795–816 (2004).
18. Carlson, R. L. & Miller, D. J. Mantle wedge water contents estimated from seismic velocities in partially serpentinized peridotites. *Geophys. Res. Lett.* **30,** 1250 (2003).
19. Van Avendonk, H. J. A., Holbrook, W. S., Lizarralde, D. & Denyer, P. Structure and serpentinization of the subducting Cocos plate offshore Nicaragua and Costa Rica. *Geochem. Geophys. Geosyst.* **12,** Q06009 (2011).
20. Kirby, S. H., Stein, S., Okal, E. A. & Rubie, D. C. Metastable mantle phase transformations and deep earthquakes in subducting oceanic lithosphere. *Rev. Geophys.* **34,** 261–306 (1996).
21. van Keken, P. E., Hacker, B. R., Syracuse, E. M. & Abers, G. A. Subduction factory 4: Depth-dependent flux of H_2O from subduction slabs worldwide. *J. Geophys. Res.* **116,** B01401 (2011).
22. Jiao, W., Silver, P. G., Fei, Y. & Prewitt, C. T. Do intermediate- and deep-focus earthquakes occur on pre-existing weak zones? An examination of the Tonga subduction zone. *J. Geophys. Res.* **105,** 28125–128138 (2000).
23. Ranero, C. R., Villaseñor, A., Morgan, J. P. & Weinrebe, W. Relationship between bend-faulting at trenches and intermediate depth seismicity. *Geochem. Geophys. Geosyst.* **6,** Q12002 (2005).
24. Kelemen, P. B. & Hirth, G. A periodic shear-heating mechanism for intermediate-depth earthquakes in the mantle. *Nature* **446,** 787–790 (2007).
25. Ruff, L. J. Do trench sediments affect great earthquake occurrence in subduction zones? *Pageoph* **129,** 263–282 (1989).
26. Scholz, C. H. & Small, C. The effect of seamount subduction on seismic coupling. *Geology* **25,** 487–490 (1997).
27. Scholz, C. H. *The Mechanics of Earthquakes and Faulting* (Cambridge Univ, Press, 1990).
28. Saffer, D. M. & Tobin, H. J. Hydrogeology and mechanics of subduction zone forearcs: Fluid flow and pore pressure. *Ann. Rev. Earth Planet. Sci.* **39,** 157–186 (2011).
29. Maus, S. *et al.* EMAG2: A 2-arc min resolution Earth magnetic anomaly grid compiled from satellite, airborne, and marine magnetic measurements. *Geochem. Geophys. Geosyst.* **10,** Q08005 (2009).
30. Bird, P. An updated digital model of plate boundaries. *Geochem. Geophys. Geosyst.* **4,** 1027 (2003).

Acknowledgements

We gratefully acknowledge the captain, technical staff and crew of the RV *Marcus G. Langseth* and the Scripps OBS team, who made this data set possible through their remarkable dedication in a challenging environment. This work was supported by the National Science Foundation. We thank J. Gaherty and N. Miller for helpful feedback.

Author contributions

D.J.S., M.R.N. and S.C.W. obtained financial support for the marine seismic programme, and G.A.A., K.M.K. and D.J.S. obtained financial support for onshore seismic deployment through NSF grants. D.J.S., A.B., M.R.N., H.K., S.C.W., J.L. and M.D. collected marine data during a research cruise on RV *Langseth*, and K.M.K. and D.J.S. deployed and recovered onshore seismometers. D.J.S., A.B., M.R.N., H.K. and J.L. analysed marine seismic data, and D.J.S., G.A.A., K.M.K. and G.A.M.-S. analysed seismicity data. D.J.S. wrote the manuscript with contributions from all other authors.

Additional information

Supplementary information is available in the online version of the paper. Reprints and permissions information is available online at www.nature.com/reprints. Correspondence and requests for materials should be addressed to D.J.S.

Competing financial interests

The authors declare no competing financial interests.

Methods

Multichannel seismic (MCS) reflection data. MCS data were acquired using two 8-km-long seismic streamers separated by 450 m and towed at 9 and 12 m depth, respectively. Each streamer was composed of 636 receiver-array groups spaced at 12.5 m, for a total recording of 1,272 channels per shot. Data were recorded for 18 or 22 s at a 2-ms sample rate. The seismic source was the 6,600 cu. in. tuned 36-element airgun array of the RV *Marcus G. Langseth* towed at 12 m depth. Data processing steps consisted of binning, band-pass filtering and noise suppression using the LIFT method[31], predictive deconvolution, velocity analysis, normal moveout, stacking and post-stack Kirchhoff time migration using Paradigm Geophysical software. For this work, we analyse only data from the deeper streamer.

Bathymetry data. Multibeam bathymetry data were acquired with a Kongsberg EM 122 system aboard the RV *Marcus G. Langseth*. Swath widths were 12–15 km at water depths >4.5 km. Basic onboard swath processing was done using MB-system[32], and consisted of automatic removal of spikes and excessive slopes followed by manual ping editing. The cleaned pings were gridded with a 100-m grid spacing. Bathymetry data were used to characterize the orientation of bending faults and their throws at the surface over the western part of the study area, where bending faulting is abundant, to illuminate possible controls on faulting. Around and east of Line 3 (outboard of the Semidi segment), bending faults are not clearly identifiable in the bathymetry data. See Supplementary Methods for more information on analysis of bathymetry data.

Wide-angle seismic reflection/refraction data. Wide-angle seismic refraction data were acquired using the four-component, short-period ocean-bottom seismometers from Scripps Institution of Oceanography spaced at ~15 km along two ~300-km-long profiles. The source of seismic energy was the same as for the MCS surveying, but a longer shot interval (90 s) was used to minimize previous shot noise at longer offsets. Data processing consisted of minimum phase band-pass filtering with corners of 3–5–15–20 Hz and application of offset varying gains. We used regularized tomographic inversion of travel-time picks using Jive3D (ref. 33) to create models of P-wave velocity from the subset of data that constrained the downgoing plate. In the final models, layers are included for the water column, sediments, oceanic and continental crust, and oceanic mantle. Picks from MCS profiles of the basement and base of the crust were used to provide additional constraints on interface geometry. Travel-time picks have uncertainties of 50–125 ms. Grid spacing is 1×0.5 km in the crust and 2×1 km in the mantle. Smoothing constraints are set to apply a factor of 2 more horizontal than vertical smoothing, and allow a factor of 3 more interface roughness than velocity roughness. Line 5 has an r.m.s. misfit of 86 ms and a chi-squared misfit of 1.19. Line 3 has an r.m.s. misfit of 98 ms and a chi-squared misfit of 1.07. More information on OBS data, tests of velocity models, and model interpretation can be found in the Supplementary Methods.

Seismicity. To quantify variations in seismicity along this part of the Alaska subduction zone, we compare the number of earthquakes within several depth ranges in the Alaska Earthquake Information Center (AEIC) catalogue since 1990, and compare them with the EHB catalogue[34], and a local catalogue for a two-month temporary deployment in the summer of 2011, during the controlled-source seismic experiment. For each of these catalogues, we counted the events north of the trench within a moving bin oriented in the convergence direction occurring at depth intervals from 0–50 km, 50–100 km, and greater than 100 km. One-degree-wide bins were chosen for the AEIC catalogue, which capture the ~100-km wavelength variations in seismicity that are relevant for this study. Only events north of the trench were included so that outer-rise events were omitted. To examine variations in outer-rise seismicity, we also counted events within the same bins south of the trench in all depth ranges. All catalogues show the same pattern, where fewer events are observed in all depth ranges within the Semidi segment than in the Shumagin Gap. See Supplementary Methods for more information.

Data and code availability. All ALEUT seismic and bathymetric data are available through the Marine Geoscience Data System (http://www.marine-geo.org/tools/search/entry.php?id=MGL1110). Earthquake catalogues are available online for the AEIC (http://www.aeic.alaska.edu) and EHB (http://www.isc.ac.uk/ehbbulletin). Data from the temporary local network are available from Incorporated Research Institutions for Seismology (http://ds.iris.edu/ds). Both of the tomography codes employed in this study are available online (JIVE3D (ref. 33), http://bullard.esc.cam.ac.uk/ĥobro/Jive3D; TOMO2D (ref. 35), http://people.earth.yale.edu/software/jun-korenaga).

References

31. Choo, J., Downton, J. & Dewar, J. LIFT: A new and practical approach to noise and multiple attenuation. *First Break* **22,** 39–43 (2004).
32. Caress, D. W. & Chayes, D. N. in *Proc. of the IEEE Oceans 95 Conf.* 997–1000 (MTS/IEEE, 1995).
33. Hobro, J. W. D., Singh, S. C. & Minshull, T. A. Three-dimensional tomographic inversion of combined reflection and refraction seismic traveltime data. *Geophys. J. Int.* **152,** 79–93 (2003).
34. Engdahl, E. R., van der Hilst, R. & Buland, R. Global teleseismic earthquake relocation with improved travel times and procedures for depth determination. *Bull. Seismol. Soc. Am.* **88,** 722–743 (1998).
35. Korenaga, J. *et al.* Crustal structure of the southeast Greenland margin from joint refraction and reflection seismic tomography. *J. Geophys. Res.* **105,** 21591–521614 (2000).